# Novel Quasi-Direct Rotor Position Estimator for Permanent Magnet Synchronous Machines based on the Back-Electromotive Force using Current Oversampling

Georg Lindemann, Viktor Willich and Axel Mertens
Leibniz University Hannover
Institute for Drive Systems and Power Electronics
Welfengarten 1
Hannover, Germany
Email: georg.lindemann@ial.uni-hannover.de
URL: https://www.ial.uni-hannover.de

## Acknowledgments

This work was supported by the German Research Foundation (DFG) - Project 329209868.

## Keywords

≪Self-sensing control≫, ≪Current derivative≫, ≪Field programmable gate array (FPGA)≫, ≪Permanent magnet motor≫.

## Abstract

This paper presents an approach for rotor position estimation in permanent magnet synchronous machines (PMSMs) based on back-electromotive force (EMF). By directly evaluating the voltage equation and using current oversampling, highly responsive dynamics can be achieved. Online optimisation ensures an analytically adjustable, quasi-direct calculation of the rotor position.

## Introduction

In the past, different methods for rotor position estimation in PMSMs have been presented [1]. The estimation methods can be divided into methods for low speeds and standstill and methods for higher speeds. The methods used for higher speeds are based on the EMF of the machine. The proposed EMF-based method should first be classified according to the current state of research. Conventional methods are based on the evaluation of the current measurement and voltage setpoints of the converter once per pulse width modulation (PWM) period. Direct calculation of the EMF in the stator reference frame is possible, but additional filters are needed for estimated position and speed [2]. The evaluation of the EMF in the estimated rotor reference frame takes advantage of handling direct quantities. For interior PMSMs, the approach of extended EMF has been established, which considers the fact that the EMF is dependent not only on the induced voltage from the permanent magnet (PM) but also to the stator inductances [3]. The extended EMF also considers the positional information given by the magnetic saliency. Despite the additional considerations of this approach, the magnetic saturation effects and non-linearity of the machine are neglected. The proposed method bridges this gap as it is derived by using the non-linear differential equation of the PMSM to estimate the rotor position with a high accuracy at high-saturation operating points.

The methods based on the magnetic anisotropy of the machine, which are applied in the lower speed range and at zero speed, have been improved. Here, it is worth highlighting the flux derivative estimator quasi-direct (FDE-QD) presented in [4–6], which shows the dynamics of the closed-loop self-sensing control (SSC) of a PMSM coupled to an encoder-based control. The method utilises the advantages of current oversampling (sampling of 100 measured values during a PWM period) [7, 8] and requires a square-wave injection (SWI) along the estimated $\hat{\mathrm{d}}$-axis of the PMSM [9]. This motivates the development of a method based on a similar estimator structure for the middle and high speed ranges that does not require a test signal and still offers the highly responsive dynamics and accuracy of rotor position estimation. A test signal is no longer necessary in the higher speed range as the EMF becomes

greater and can thus be evaluated. Therefore the proposed method is named the back-electromotive force estimator quasi-direct (EMF-QD).
Estimation methods based on a current or flux observer require all machine parameters and are limited in their dynamics [10], whereas EMF-QD has fewer parameter dependencies and offers good dynamics. By evaluating the voltage equation during a passive switching state (PS) of the converter, the estimation becomes independent from the value of the output voltages of the inverter. By simplifying the optimisation algorithm of the EMF-QD, independence from the value of the permanent magnet flux linkage can be achieved.
The introduction of the EMF-QD brings the possibility of self-sensing control in highly saturated machines with highly active control dynamics, which offers a major advantage over conventional EMF-based approaches.
For the FDE-QD, the use of current oversampling and the evaluation of individual switching states of the inverter makes a vast difference to the dynamics achieved. In order to use these advantages in higher speed ranges, the EMF-QD also utilizes the current oversampling. Therefore the discrete converter voltages are evaluated and the position estimation can be examined individually in one PWM period. A similar method based on current oversampling was presented in [11]. An essential difference of [11] is the linearisation of the voltage equation by assuming the inductance values to be saturation independent. Another significant difference of [11] is the evaluation of the voltage equation, as described below, which gives the estimate a high dynamic range with good noise behaviour while all parameters can be set analytically.
The voltage differential equation of the PMSM, used as the basis for the EMF-QD, results in a voltage prediction error which can be transferred into a rotation of the dq-coordinate reference frame. Since this voltage error is minimised within one calculation period (quasi-directly), the method is, in general, able to provide a significantly better dynamic response in the rotor position estimation than a method which minimises the estimation error over several calculation steps. The calculation of the rotor position and speed according to [5] provides a structure that can be parameterised analytically and does not need to be adjusted by experiment. This provides a major advantage over methods that use a phase-locked loop (PLL) for estimation and have to be tuned by experiment [10–12].
The first section of this paper describes the mathematical principles behind minimising the estimation error and derives the basic error equation for the estimation method on the basis of the voltage differential equation of the PMSM. Next, the implemented estimation structure is described, and in the third section, the estimation method is examined in simulations and experiments.

# Non-linear Model of the PMSM

The voltage equation of the PMSM can be expressed as the sum of an ohmic part and a voltage that is induced by the derivative of the flux. The voltage equation in the stator-fixed $\alpha\beta$-reference frame is:

$$\vec{u}_{\alpha\beta} = R\vec{i}_{\alpha\beta} + \frac{\mathrm{d}\vec{\Psi}_{\alpha\beta}}{\mathrm{d}t}. \tag{1}$$

The stator resistance $R$ is considered to be isotropic. The vectors $\vec{i}_{\alpha\beta}$ and $\vec{\Psi}_{\alpha\beta}$ are the vectors of the stator currents and flux linkage in the $\alpha\beta$-reference frame, respectively. The flux linkage can be expressed in rotor-fixed dq-coordinates with the help of the electrical rotor position $\gamma_{\mathrm{el}}$:

$$\begin{aligned} \vec{u}_{\alpha\beta} &= R\vec{i}_{\alpha\beta} + \frac{\mathrm{d}\mathbf{T}\vec{\Psi}_{\mathrm{dq}}}{\mathrm{d}t} \\ &= R\vec{i}_{\alpha\beta} + \mathbf{T}\frac{\mathrm{d}\vec{\Psi}_{\mathrm{dq}}}{\mathrm{d}t} + \frac{\mathrm{d}\mathbf{T}}{\mathrm{d}t}\vec{\Psi}_{\mathrm{dq}} \\ &= R\vec{i}_{\alpha\beta} + \mathbf{T}\frac{\mathrm{d}\vec{\Psi}_{\mathrm{dq}}}{\mathrm{d}\vec{i}_{\mathrm{dq}}}\frac{\mathrm{d}\vec{i}_{\mathrm{dq}}}{\mathrm{d}t} + \mathbf{J}\omega_{\mathrm{el}}\mathbf{T}\vec{\Psi}_{\mathrm{dq}} \end{aligned} \tag{2}$$

with

$$\mathbf{T} = \begin{pmatrix} \cos(\gamma_{\mathrm{el}}) & -\sin(\gamma_{\mathrm{el}}) \\ \sin(\gamma_{\mathrm{el}}) & \cos(\gamma_{\mathrm{el}}) \end{pmatrix}, \quad \omega_{\mathrm{el}} = \frac{\mathrm{d}\gamma_{\mathrm{el}}}{\mathrm{d}t}, \quad \mathbf{J} = \begin{pmatrix} 0 & -1 \\ 1 & 0 \end{pmatrix} \tag{3}$$

The deviation of the flux linkage caused by the currents is introduced as the differential inductance matrix $\mathbf{L}'_{\mathrm{dq}}$ which is described in Equation (4). The flux linkage can be separated into one part that is dependent on the permanent magnet and another part dependent on the stator current (6). The current-dependent part is defined as $\mathbf{L}_{\mathrm{dq}}\vec{i}_{\mathrm{dq}}$, where $\mathbf{L}_{\mathrm{dq}}$ represents the secant inductance matrix as defined in (5).

$$\mathbf{L}_{\mathrm{dq}}^{'} := \frac{\mathrm{d}\vec{\Psi}_{\mathrm{dq}}}{\mathrm{d}\vec{i}_{\mathrm{dq}}} = \begin{pmatrix} L_{\mathrm{d}}^{'}(\vec{i}_{\mathrm{dq}}) & L_{\mathrm{dq}}^{'}(\vec{i}_{\mathrm{dq}}) \\ L_{\mathrm{dq}}^{'}(\vec{i}_{\mathrm{dq}}) & L_{\mathrm{q}}^{'}(\vec{i}_{\mathrm{dq}}) \end{pmatrix} \tag{4}$$

$$\mathbf{L}_{\mathrm{dq}} := \begin{pmatrix} L_{\mathrm{d}}(\vec{i}_{\mathrm{dq}}) & L_{\mathrm{dq}}(\vec{i}_{\mathrm{dq}}) \\ L_{\mathrm{dq}}(\vec{i}_{\mathrm{dq}}) & L_{\mathrm{q}}(\vec{i}_{\mathrm{dq}}) \end{pmatrix} \tag{5}$$

$$\vec{\Psi}_{\mathrm{dq}} = \vec{\Psi}_{\mathrm{L,dq}} + \vec{\Psi}_{\mathrm{PM,dq}} = \mathbf{L}_{\mathrm{dq}}\vec{i}_{\mathrm{dq}} + \Psi_{\mathrm{PM}} \begin{pmatrix} 1 \\ 0 \end{pmatrix} \tag{6}$$

The voltage equation in the $\alpha\beta$-reference frame can be derived from equations (4), (6) and (5) is given in (7).

$$\vec{u}_{\alpha\beta} = R\vec{i}_{\alpha\beta} + \mathbf{T}\mathbf{L}_{\mathrm{dq}}^{'}\frac{\mathrm{d}\vec{i}_{\mathrm{dq}}}{\mathrm{d}t} + \mathbf{J}\omega_{\mathrm{el}}\mathbf{T}\mathbf{L}_{\mathrm{dq}}\vec{i}_{\mathrm{dq}} + \mathbf{J}\omega_{\mathrm{el}}\mathbf{T}\vec{\Psi}_{\mathrm{PM,dq}} \tag{7}$$

Transforming all parameters into the $\alpha\beta$-reference frame using the product rule for the derivation of $\mathbf{T}^{-1}\vec{i}_{\alpha\beta}$ and the transformation of the inductances with $\mathbf{L}_{\alpha\beta}^{'} = \mathbf{T}\mathbf{L}_{\mathrm{dq}}^{'}\mathbf{T}^{-1}$ and $\mathbf{L}_{\alpha\beta} = \mathbf{T}\mathbf{L}_{\mathrm{dq}}\mathbf{T}^{-1}$, the non-linear differential equation yields:

$$\vec{u}_{\alpha\beta} = R\vec{i}_{\alpha\beta} + \mathbf{L}_{\alpha\beta}^{'}\frac{\mathrm{d}\vec{i}_{\alpha\beta}}{\mathrm{d}t} + \left(\mathbf{J}\mathbf{L}_{\alpha\beta} - \mathbf{L}_{\alpha\beta}^{'}\mathbf{J}\right)\omega_{\mathrm{el}}\vec{i}_{\alpha\beta} + \mathbf{J}\omega_{\mathrm{el}}\vec{\Psi}_{\mathrm{PM},\alpha\beta}. \tag{8}$$

By using Equation (8), the saturation dependence of the inductances is taken into account and can be used in the following to derive the estimation structure.

# Derivation of Rotor Position Estimation Method

In this section, the optimisation method is presented and the error equation used for rotor position estimation is derived.

## gradient descent method

The proposed estimator uses an online optimisation method based on the gradient descent method (GDM) and analogous to FDE-QD [4] to minimise a cost function. The variable of the GDM is the estimated rotor position estimation error $\hat{\gamma}_{\mathrm{err}} = \gamma_{\mathrm{el}} - \hat{\gamma}_{\mathrm{el}}$, with $\hat{\gamma}_{\mathrm{el}}$ being the estimated rotor position. The cost function (9) is defined and minimised by proceeding iteratively in the direction of the negative gradient of this function (10) [13].

$$E = \frac{1}{2}\vec{e}(\hat{\gamma}_{\mathrm{err}})^{T}\vec{e}(\hat{\gamma}_{\mathrm{err}}) \tag{9}$$

$$g = \vec{e}^{\,T}(\hat{\gamma}_{\mathrm{err}})\frac{\partial\vec{e}(\hat{\gamma}_{\mathrm{err}})}{\partial\hat{\gamma}_{\mathrm{err}}} \tag{10}$$

The result of one iterative step can be expressed as:

$$\hat{\gamma}_{\mathrm{err}}(k+1) = \hat{\gamma}_{\mathrm{err}}(k) - \eta \cdot \mathrm{sign}(g(k)). \tag{11}$$

The step-width of the GDM is $\eta$ . The error equation $\vec{e}_{\mathrm{EMF\text{-}QD},\hat{\mathrm{dq}}}(\hat{\gamma}_{\mathrm{err}})$ is derived below.

## Error Equation EMF-QD

The use of the current oversampling offers the possibility of measuring the current slopes of each switching state in stator-fixed coordinates. However, when these measured slopes are transformed into the rotating reference frame using the transformation matrix $\mathbf{T}$, the resulting values do not represent the real current slopes in the rotating dq-reference frame. This is due to the change in rotor position during each individual switching state. This deviation in the rotor position can be neglected at standstill and in low speed operation. At higher speed this would introduce an additional error into the estimation and therefore needs to be considered. The solution to consider this error is the interpretation of the current derivative $\frac{\mathrm{d}}{\mathrm{d}t}\vec{i}_{\alpha\beta}$ as a measured value $\vec{\xi}_{\alpha\beta}$.

$$\frac{\mathrm{d}\vec{i}_{\alpha\beta}}{\mathrm{d}t} = \vec{\xi}_{\alpha\beta} \tag{12}$$

Inserting this relationship into Equation (8) and transforming it into the rotating $dq$-reference frame results in:

$$\vec{u}_{\mathrm{dq}} = \mathbf{T}^{-1}R\vec{i}_{\alpha\beta} + \mathbf{T}^{-1}\mathbf{L}_{\alpha\beta}^{'}\vec{\xi}_{\alpha\beta} + \mathbf{T}^{-1}\left(\mathbf{J}\mathbf{L}_{\alpha\beta} - \mathbf{L}_{\alpha\beta}^{'}\mathbf{J}\right)\omega_{\mathrm{el}}\vec{i}_{\alpha\beta} + \mathbf{T}^{-1}\mathbf{J}\omega_{\mathrm{el}}\vec{\Psi}_{\mathrm{PM},\alpha\beta}. \tag{13}$$

If all values are transformed from the αβ-reference frame into the dq-reference frame, the equation (14) results when considering the current gradients as measured values. This equation takes into account the non-linearity of the inductance matrix $\mathbf{L}'_{\mathrm{dq}}$.

$$\vec{u}_{\mathrm{dq}} = R\vec{i}_{\mathrm{dq}} + \mathbf{L}'_{\mathrm{dq}}\vec{\xi}_{\mathrm{dq}} + \left(\mathbf{J}\mathbf{L}_{\mathrm{dq}} - \mathbf{L}'_{\mathrm{dq}}\mathbf{J}\right)\omega_{\mathrm{el}}\vec{i}_{\mathrm{dq}} + \mathbf{J}\omega_{\mathrm{el}}\vec{\Psi}_{\mathrm{PM,dq}} \tag{14}$$

The estimation of the rotor position works in the rotating reference frame with the measurements in the estimated reference frame as input. To transform the variables from the $\alpha\beta$-reference frame into the estimated $\hat{\mathrm{d}}\hat{\mathrm{q}}$-reference frame, the transformation matrix $\hat{\mathbf{T}}$ is used. After inserting this into Equation (13), the voltage equation becomes (15).

$$\begin{aligned}
\vec{u}_{\mathrm{dq}} &= \mathbf{T}^{-1}R\hat{\mathbf{T}}\vec{i}_{\hat{\mathrm{d}}\hat{\mathrm{q}}} + \mathbf{T}^{-1}\mathbf{L}'_{\alpha\beta}\hat{\mathbf{T}}\vec{\xi}_{\hat{\mathrm{d}}\hat{\mathrm{q}}} + \mathbf{T}^{-1}\left(\mathbf{J}\mathbf{L}_{\alpha\beta} - \mathbf{L}'_{\alpha\beta}\mathbf{J}\right)\omega_{\mathrm{el}}\hat{\mathbf{T}}\vec{i}_{\hat{\mathrm{d}}\hat{\mathrm{q}}} + \mathbf{T}^{-1}\mathbf{J}\omega_{\mathrm{el}}\mathbf{T}\vec{\Psi}_{\mathrm{PM,dq}} \\
&= \mathbf{T}^{-1}R\hat{\mathbf{T}}\vec{i}_{\hat{\mathrm{d}}\hat{\mathrm{q}}} + \mathbf{T}^{-1}\mathbf{T}\mathbf{L}'_{\mathrm{dq}}\mathbf{T}^{-1}\hat{\mathbf{T}}\vec{\xi}_{\hat{\mathrm{d}}\hat{\mathrm{q}}} + \mathbf{T}^{-1}\mathbf{T}\left(\mathbf{J}\mathbf{L}_{\mathrm{dq}} - \mathbf{L}'_{\mathrm{dq}}\mathbf{J}\right)\mathbf{T}^{-1}\omega_{\mathrm{el}}\hat{\mathbf{T}}\vec{i}_{\hat{\mathrm{d}}\hat{\mathrm{q}}} + \mathbf{T}^{-1}\mathbf{J}\omega_{\mathrm{el}}\mathbf{T}\vec{\Psi}_{\mathrm{PM,dq}} \\
&= R\tilde{\mathbf{T}}\vec{i}_{\hat{\mathrm{d}}\hat{\mathrm{q}}} + \mathbf{L}'_{\mathrm{dq}}\tilde{\mathbf{T}}\vec{\xi}_{\hat{\mathrm{d}}\hat{\mathrm{q}}} + \left(\mathbf{J}\mathbf{L}_{\mathrm{dq}} - \mathbf{L}'_{\mathrm{dq}}\mathbf{J}\right)\omega_{\mathrm{el}}\tilde{\mathbf{T}}\vec{i}_{\hat{\mathrm{d}}\hat{\mathrm{q}}} + \mathbf{J}\omega_{\mathrm{el}}\vec{\Psi}_{\mathrm{PM,dq}}
\end{aligned} \tag{15}$$

with

$$\hat{\mathbf{T}} = \begin{pmatrix} \cos(\hat{\gamma}_{\mathrm{el}}) & -\sin(\hat{\gamma}_{\mathrm{el}}) \\ \sin(\hat{\gamma}_{\mathrm{el}}) & \cos(\hat{\gamma}_{\mathrm{el}}) \end{pmatrix} \qquad \tilde{\mathbf{T}} = \mathbf{T}^{-1}\hat{\mathbf{T}} = \begin{pmatrix} \cos(\gamma_{\mathrm{err}}) & \sin(\gamma_{\mathrm{err}}) \\ -\sin(\gamma_{\mathrm{err}}) & \cos(\gamma_{\mathrm{err}}) \end{pmatrix} \tag{16}$$

Figure 1 shows an example progression of voltage and current along the estimated $\hat{\mathrm{d}}$-axis during a PWM period.

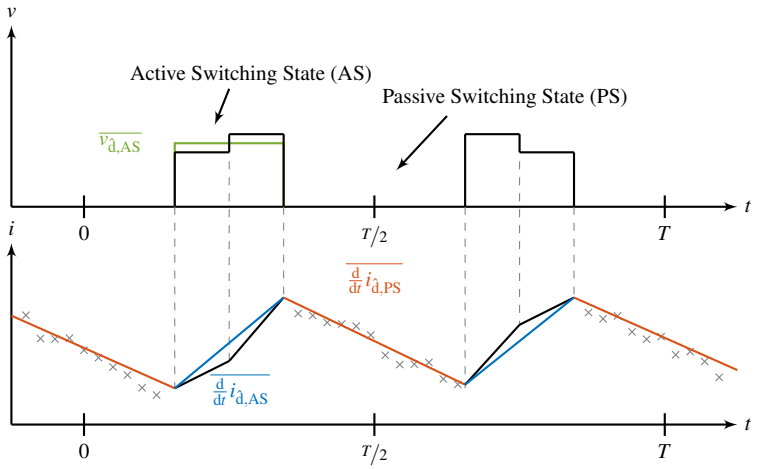


Fig. 1: Example voltage and current progression during a PWM period

By using current oversampling, many current measured values are available during one PWM period. By applying a least mean squares (LMS) algorithm during the PS, the slopes and mean values during active switching state (AS) and PS of the converter can be determined. To decouple the estimation algorithm from mapping errors of the converter voltage, Equation (15) is evaluated during the PS ($\vec{u}_{\mathrm{dq,PS}} = 0$). The error equation during a PS is thus:

$$\vec{e}_{\mathrm{EMF\text{-}QD},\hat{\mathrm{d}}\hat{\mathrm{q}}} = R\tilde{\mathbf{T}}\overline{\vec{i}_{\hat{\mathrm{d}}\hat{\mathrm{q}},\mathrm{PS}}} + \mathbf{L}'_{\mathrm{dq}}\tilde{\mathbf{T}}\overline{\vec{\xi}_{\hat{\mathrm{d}}\hat{\mathrm{q}},\mathrm{PS}}} + \left(\mathbf{J}\mathbf{L}_{\mathrm{dq}} - \mathbf{L}'_{\mathrm{dq}}\mathbf{J}\right)\omega_{\mathrm{el}}\tilde{\mathbf{T}}\overline{\vec{i}_{\hat{\mathrm{d}}\hat{\mathrm{q}},\mathrm{PS}}} + \mathbf{J}\omega_{\mathrm{el}}\vec{\Psi}_{\mathrm{PM,dq}} \tag{17}$$

## Implementation

To find the error equation of the GDM, the $\hat{\mathrm{d}}$-axis of the voltage equation is considered. It is assumed that the method is in steady state and therefore $\omega_{\mathrm{el}} \approx \hat{\omega}_{\mathrm{el}}$ applies. By linearisation, the error equation can be derived:

$$\begin{aligned}
e_{\mathrm{EMF\text{-}QD},\hat{\mathrm{d}}} = {} & \check{R}\left(\overline{i_{\hat{\mathrm{d}},\mathrm{PS}}} + \hat{\gamma}_{\mathrm{err}}\overline{i_{\hat{\mathrm{q}},\mathrm{PS}}}\right) + \left(\check{L}'_{\mathrm{d}} - \check{L}'_{\mathrm{dq}}\hat{\gamma}_{\mathrm{err}}\right)\overline{\xi_{\hat{\mathrm{d}},\mathrm{PS}}} + \left(\check{L}'_{\mathrm{d}}\hat{\gamma}_{\mathrm{err}} + \check{L}'_{\mathrm{dq}}\right)\overline{\xi_{\hat{\mathrm{q}},\mathrm{PS}}} \\
& + \left[\left(\check{L}'_{\mathrm{d}} - \check{L}_{\mathrm{q}}\right)\left(\overline{i_{\hat{\mathrm{q}},\mathrm{PS}}} - \overline{i_{\hat{\mathrm{d}},\mathrm{PS}}}\hat{\gamma}_{\mathrm{err}}\right) - \left(\check{L}_{\mathrm{dq}} + \check{L}'_{\mathrm{dq}}\right)\left(\overline{i_{\hat{\mathrm{d}},\mathrm{PS}}} + \overline{i_{\hat{\mathrm{q}},\mathrm{PS}}}\hat{\gamma}_{\mathrm{err}}\right)\right]\hat{\omega}_{\mathrm{el}}.
\end{aligned} \tag{18}$$

With regard to the implementation, the parameters of the PMSM are expressed by measured values, as they may contain parameter errors. These are indicated by a superscripted $\check{}$. Furthermore, it should be noted that $\gamma_{\mathrm{err}}$ is replaced by $\hat{\gamma}_{\mathrm{err}}$. $\hat{\gamma}_{\mathrm{err}}$ denotes the estimated disorientation of the $\hat{\mathrm{d}}\hat{\mathrm{q}}$-reference frame, which corresponds to $\gamma_{\mathrm{err}}$ in ideal function. With the help of (19), the gradient (20) can be formulated.

$$\frac{\partial e_{\text{EMF-QD},\hat{\mathrm{d}}}}{\partial \hat{\gamma}_{\mathrm{err}}} = \check{R}\overline{i_{\hat{\mathrm{q}},\mathrm{PS}}} + \check{L}'_{\mathrm{d}}\overline{\xi_{\hat{\mathrm{q}},\mathrm{PS}}} - \left(\left(\check{L}'_{\mathrm{d}} - \check{L}_{\mathrm{q}}\right)\overline{i_{\hat{\mathrm{d}},\mathrm{PS}}} + \left(\check{L}_{\mathrm{dq}} + \check{L}'_{\mathrm{dq}}\right)\overline{i_{\hat{\mathrm{q}},\mathrm{PS}}}\right)\hat{\omega}_{\mathrm{el}} \tag{19}$$

$$g_{\text{EMF-QD}} = e_{\text{EMF-QD},\hat{\mathrm{d}}}\frac{\partial e_{\text{EMF-QD},\hat{\mathrm{d}}}}{\partial \hat{\gamma}_{\mathrm{err}}} \tag{20}$$

Equation (19) is examined below for the dependence of the terms. For this purpose, the value $\overline{\xi_{\hat{\mathrm{q}},\mathrm{PS}}}$ is substituted by ideal values using Equation (13) during the PS:

$$\begin{aligned}\overline{\xi_{\hat{\mathrm{q}},\mathrm{PS}}} \overset{\hat{\gamma}_{\mathrm{err}}\to 0}{=} \overline{\xi_{\mathrm{q},\mathrm{PS}}} &= -\frac{1}{L'_{\mathrm{q}}}\left[R\overline{i_{\mathrm{q},\mathrm{PS}}} + \overline{\xi_{\mathrm{d},\mathrm{PS}}}L'_{\mathrm{dq}}\right. \\ &\quad \left. + \left(\left(L_{\mathrm{d}} - L'_{\mathrm{q}}\right)\overline{i_{\mathrm{d},\mathrm{PS}}} - \left(L_{\mathrm{dq}} + L'_{\mathrm{dq}}\right)\overline{i_{\mathrm{q},\mathrm{PS}}}\right)\omega_{\mathrm{el}} + \omega_{\mathrm{el}}\Psi_{\mathrm{PM}}\right].\end{aligned} \tag{21}$$

For the dependence on parameters and with regard to a lower speed limit $\omega_{\mathrm{el,min}}$, (19) results in

$$\begin{aligned}\left(\frac{\partial e_{\text{EMF-QD},\hat{\mathrm{d}}}}{\partial \hat{\gamma}_{\mathrm{err}}}\right)_{\mathrm{para}} &= R\overline{i_{\mathrm{q},\mathrm{PS}}}\left(1 - \frac{L'_{\mathrm{d}}}{L'_{\mathrm{q}}}\right) - \frac{L'_{\mathrm{d}}}{L'_{\mathrm{q}}}\overline{\xi_{\mathrm{d},\mathrm{PS}}}L'_{\mathrm{dq}} - \frac{L'_{\mathrm{d}}}{L'_{\mathrm{q}}}(L'_{\mathrm{d}} - L_{\mathrm{q}})\overline{i_{\mathrm{d},\mathrm{PS}}}\omega_{\mathrm{el,min}} \\ &\quad + \frac{L'_{\mathrm{d}}}{L'_{\mathrm{q}}}(L_{\mathrm{dq}} + L'_{\mathrm{dq}})\overline{i_{\mathrm{q},\mathrm{PS}}}\omega_{\mathrm{el,min}} - \frac{L'_{\mathrm{d}}}{L'_{\mathrm{q}}}\Psi_{\mathrm{PM}}\omega_{\mathrm{el,min}} - (L'_{\mathrm{d}} - L_{\mathrm{q}})\overline{i_{\mathrm{d},\mathrm{PS}}}\omega_{\mathrm{el,min}} \\ &\quad - (L_{\mathrm{d}} - L'_{\mathrm{q}})\overline{i_{\mathrm{d},\mathrm{PS}}}\omega_{\mathrm{el,min}}.\end{aligned} \tag{22}$$

Next, the operating range in which (22) depends on the value of the induced voltage is determined in a simplified way. To figure out this operating range, $\overline{i_{\mathrm{d},\mathrm{PS}}} = 0$ is set as the worst-case estimate. This results in the minimum speed at which the term of the induced voltage dominates:

$$\left|\omega_{\mathrm{el,min}}\right| = \left|\frac{\overline{\xi_{\mathrm{d},\mathrm{PS}}}L'_{\mathrm{dq}} - R\overline{i_{\mathrm{q},\mathrm{PS}}}\left(\frac{L'_{\mathrm{q}}}{L'_{\mathrm{d}}} - 1\right)}{(L_{\mathrm{dq}} + L'_{\mathrm{dq}})\overline{i_{\mathrm{q},\mathrm{PS}}} - \Psi_{\mathrm{PM}}}\right|. \tag{23}$$

If the rated operating point of the machine is taken as a reference (Table I) and the mutual inductance is neglected ($L_{\mathrm{dq}} = L'_{\mathrm{dq}} = 0$), the minimum speed above which the simplified gradient applies is: $n_{\mathrm{mech,min}} \approx 128\,1/\mathrm{min}$. Above this speed, the gradient is defined by

$$g_{\text{EMF-QD,simplified}} = e_{\text{EMF-QD},\hat{\mathrm{d}}}\left(\frac{\partial e_{\text{EMF-QD},\hat{\mathrm{d}}}}{\partial \hat{\gamma}_{\mathrm{err}}}\right)_{\text{simplified}} = e_{\text{EMF-QD},\hat{\mathrm{d}}}\left(-\frac{\check{L}'_{\mathrm{d}}}{\check{L}'_{\mathrm{q}}}\hat{\omega}_{\mathrm{el}}\check{\Psi}_{\mathrm{PM}}\right). \tag{24}$$

The lower speed limit of the entire SSC using EMF-QD is identified in the experimental investigation section. Since only the sign of the gradient $g_{\text{EMF-QD,simplified}}$ is evaluated, the result of the GDM is independent of the absolute value of $\Psi_{\mathrm{PM}}$. In Figure 2, a structure for speed and position estimation analogous to that presented in [4] is shown. The termination criterion for the GDM is a fixed number of iterations. In steady-state operation, the estimation error $\hat{\gamma}_{\mathrm{err}}$ becomes 0 while the integrator part provides the estimated angular frequency $\hat{\omega}_{\mathrm{el}}$.

## Simulational and Experimental Results

In order to investigate the stability and dynamics of EMF-QD in the range of constant flux, a machine model based on the non-linear voltage equation of the PMSM is simulated. The rated data of the machine under test and related test bench data are provided in Table I. Figure 3 shows the structure of the SSC using the EMF-QD as

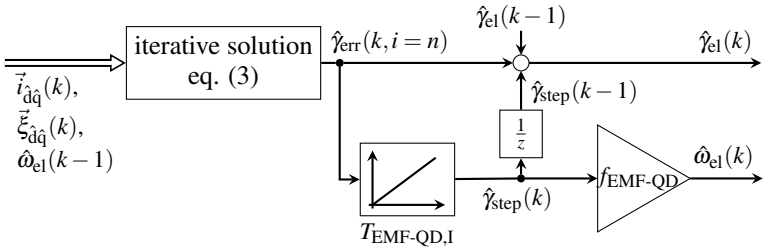


Fig. 2: Implemented structure for rotor position and speed estimation

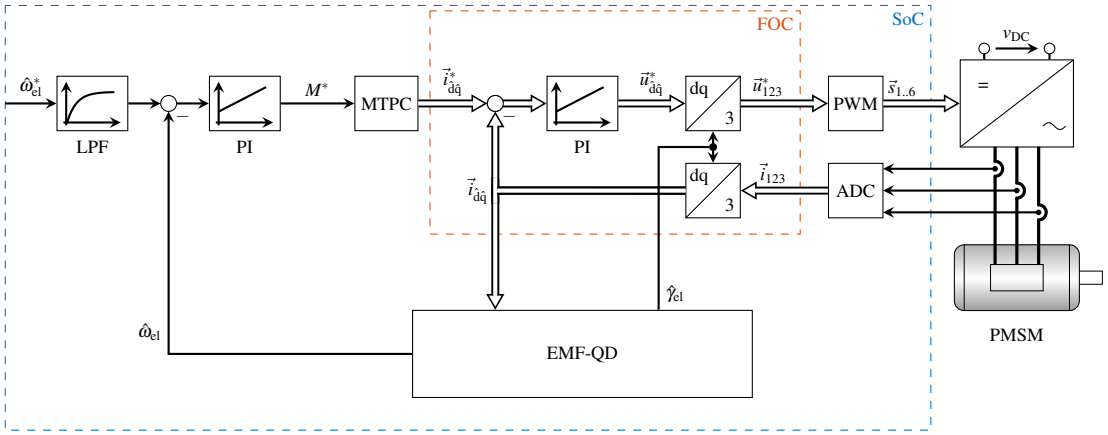


Fig. 3: Block diagram of the SSC used with PMSM and converter (encoder for benchmarking is not shown)

rotor position and speed estimator. For the investigations, closed-loop speed control is used. The speed setpoint $\hat{\omega}^*_{\mathrm{el}}$ is filtered by a first-order low-pass filter with the same time constant as the speed pi controller. The current setpoints for the field-oriented control (FOC) are derived using a maximum torque per current (MTPC) algorithm. The slopes of the measured currents are determined with an LMS algorithm during the PS using a sampling rate of 1 MSPS and are fed to the estimator. The controller and estimator parameters are given in Table II and apply to both the simulated and experimental investigations.

TABLE I
PMSM RATED VALUES AND TEST BENCH DATA

| | | |
|---|---|---|
| Rated current (RMS) | $I_{\mathrm{r}}$ | 6.7 A |
| Rated torque | $M_{\mathrm{r}}$ | 0.5 Nm |
| Rated rotational speed | $n_{\mathrm{r}}$ | 5850 $\mathrm{min}^{-1}$ |
| d-axis inductance (idle) | $L_{\mathrm{d}}$ | 198 µH |
| q-axis inductance (idle) | $L_{\mathrm{q}}$ | 255 µH |
| Phase resistance | $R$ | 0.39 Ω |
| Flux linkage | $\Psi_{\mathrm{PM}}$ | 8.05 mVs |
| Number of pole pairs | $p$ | 4 |
| DC-link voltage | $V_{\mathrm{DC}}$ | 48 V |
| PWM frequency | $f_{\mathrm{PWM}}$ | 10 kHz |

TABLE II
CONTROL PARAMETERS

| | | |
|---|---|---|
| Initial step width | $\eta_{\mathrm{EMF\text{-}QD,init}}$ | $5.2 \cdot 10^{-3}$ rad |
| Time constant EMF-QD | $T_{\mathrm{EMF\text{-}QD,N}}$ | 3 ms |
| P-gain current control | $K_{\mathrm{EMF\text{-}QD,i,P}}$ | 1.5 V/A |
| Time const. current control | $T_{\mathrm{EMF\text{-}QD,i,N}}$ | 0.5 ms |
| P-gain speed control | $K_{\mathrm{EMF\text{-}QD},\omega,\mathrm{P}}$ | 0.056 A · min |
| Time const. speed control | $T_{\mathrm{EMF\text{-}QD},\omega,\mathrm{N}}$ | 19 ms |

Two test scenarios are defined to evaluate the quality of the estimated rotor position and speed. In Figure 4, the load step response of SSC is depicted. The speed control operates at a setpoint of 1500 rpm. The load torque is set, reversed and reduced to zero. The upper plot shows the currents $i_{\hat{\mathrm{d}}}$ and $i_{\hat{\mathrm{q}}}$ in estimated coordinates followed by the estimated speed $\hat{n}_{\mathrm{mech}}$ as well as the speed setpoint $\hat{n}^*_{\mathrm{mech}}$. The speed deviation from the measured speed is defined as $n_{\mathrm{err}} = n_{\mathrm{mech}} - \hat{n}_{\mathrm{mech}}$ and depicted in the third row. The bottom line shows the rotor position estimation error $\gamma_{\mathrm{err}} = \gamma_{\mathrm{el}} - \hat{\gamma}_{\mathrm{el}}$. Figure 5 shows two setpoint steps from 1000 1/min to 2000 1/min and in the opposite direction. The two figures show that the estimation error of the EMF-QD is very small during both the dynamic process and in steady-state operation under load.

To demonstrate the stability of the method in the range of constant flux, Figure 6 shows the estimation error as a function of the load torque and speed of the PMSM. Figure 6(a) shows the root-mean-square of the estimation error

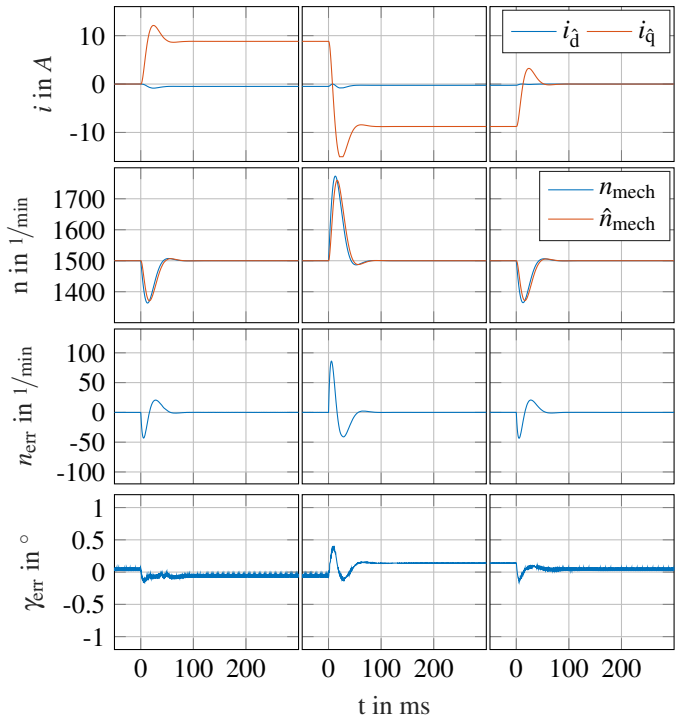


Fig. 4: Simulations of closed-loop SSC using EMF-QD with 1500 $^1/_{min}$ speed setpoint. Rated torque is applied (left), reversed (centre) and reduced to zero (right)

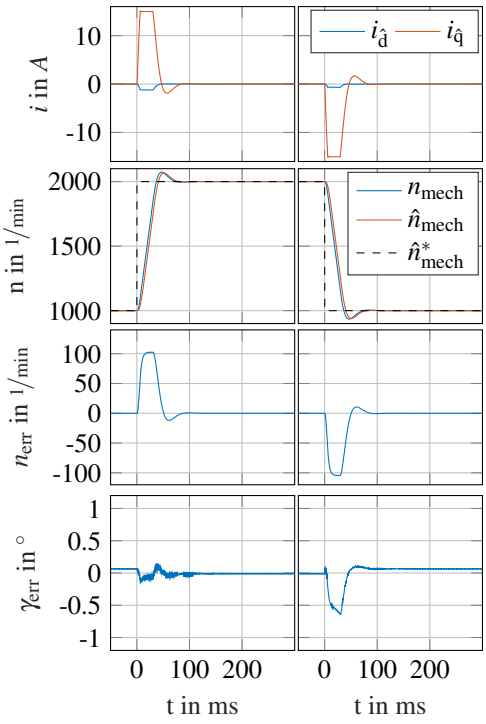


Fig. 5: Simulations of closed-loop SSC using EMF-QD. Speed setpoint is increased to 2000 $^1/_{min}$ and reduced to 1000 $^1/_{min}$

during steady-state operation, and Figure 6(b) the maximum value of the estimation error in dynamic operation. For this purpose, a step from 0 Nm to the specified load torque is performed. In the range of high inverter output levels, the error increases due to short duration of the PS and therefore leads to a reduction in the signal-to-noise ratio (SNR). In the very low speed range, the simplified gradient (10) is not valid and the SNR of the error equation is reduced.

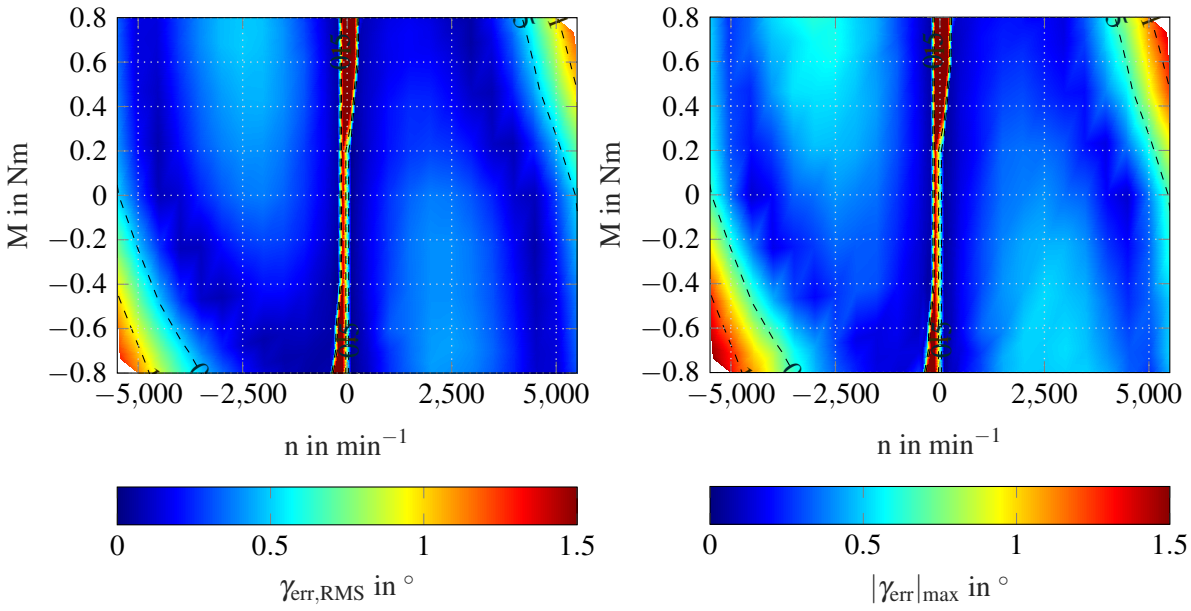


(a) RMS value in steady state

(b) Maximum value during dynamic operation

Fig. 6: Simulations of rotor position estimation error in the range of constant flux

### Experimental Results

The experimental test setup uses the rapid prototyping system IAL ControlCube, which contains a Xilinx Zynq 7000 (SoC) combining an ARM Dual Core Cortex A9 processor and an Artix-7 FPGA as programmable logic (PL). The system uses shunt-based current measurement with an A/D-converter resolution of 14 bits at a conversion frequency of 1 MSPS. The MOSFET-based inverter takes advantage of a predictive compensation method for the non-linear output voltages [14]. The test scenarios defined in simulations are repeated with the experimental test setup. The results are shown in Figure 7 and Figure 8. The measurements show a fluctuation in the estimated values due to the SNR of the current measurement and possible parameter errors. Nevertheless, the measurements show a similar shape to the simulated results and thus prove the stability and dynamic effects of the SSC on the physical system. The rotor position estimation error $\gamma_{\mathrm{err}}$ remains smaller than 9 degrees electrical across the entire range.

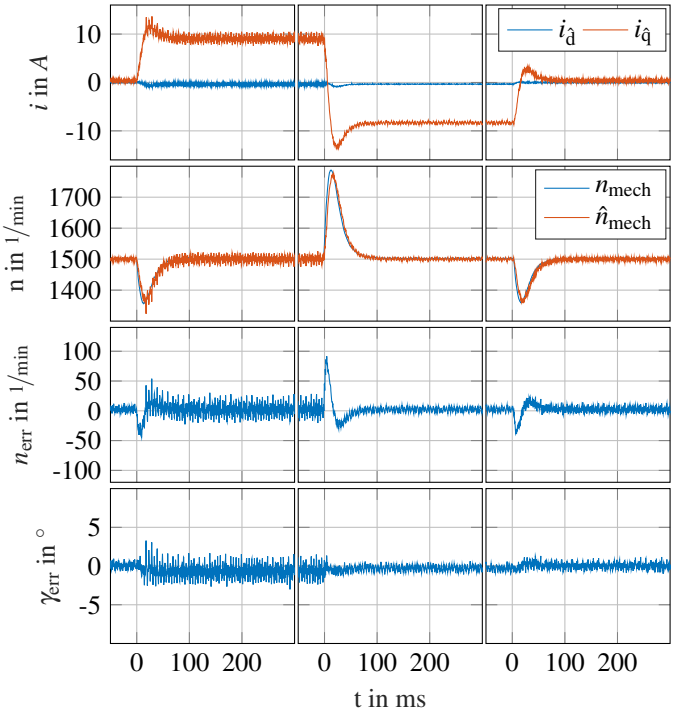


Fig. 7: Experimental results of closed-loop SSC using EMF-QD with 1500 $^{1}/_{\mathrm{min}}$ speed setpoint. Rated torque is applied (left), reversed (centre) and reduced to zero (right)

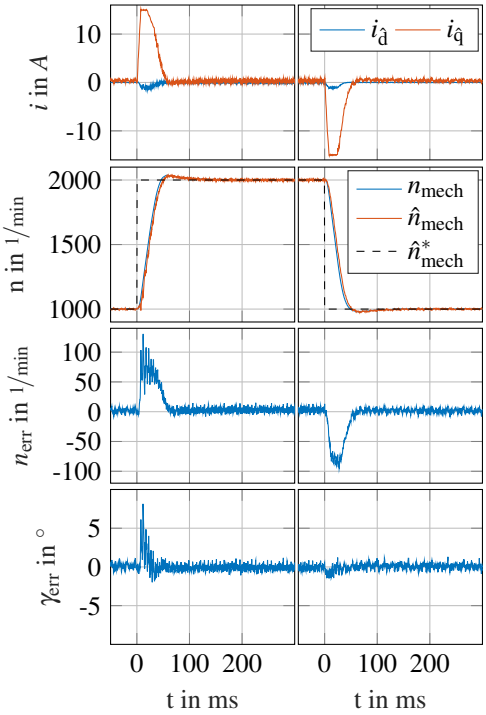


Fig. 8: Experimental results of closed-loop SSC using EMF-QD. Speed setpoint $\hat{n}^{*}_{\mathrm{mech}}$ is increased to 2000 $^{1}/_{\mathrm{min}}$ and reduced to 1000 $^{1}/_{\mathrm{min}}$

For the investigation of the lower speed limit of the EMF-QD, a speed setpoint step down to the calculated $n_{\mathrm{mech,min}}$ limit and back up to $\hat{n}^{*}_{\mathrm{mech}} = 400\,^{1}/_{\mathrm{min}}$ is shown in Fig 10. It should be noted that the dynamic response of SSC are reduced for the experiment in order to achieve lower noise in the speed estimate. The following parameters are used: $T_{\mathrm{EMF\text{-}QD,N}} = 20\,\mathrm{ms}$, $\eta_{\mathrm{EMF\text{-}QD,init}} = 31 \cdot 10^{-3}\,\mathrm{rad}$, $T_{\mathrm{EMF\text{-}QD},\omega,\mathrm{N}} = 99.7\,\mathrm{ms}$, $K_{\mathrm{EMF\text{-}QD},\omega,\mathrm{P}} = 0.011\,\mathrm{A}\cdot\mathrm{min}$. It can be seen that due to the overshoot in the estimated and measured speeds, a minimum speed of about $60\,^{1}/_{\mathrm{min}}$ is reached. This value could also be achieved in a steady state without load. The fact that the lower speed limit of the EMF-QD is below $n_{\mathrm{mech,min}}$ is reasonable because $n_{\mathrm{mech,min}}$ was calculated using a worst-case scenario at rated torque. In order to determine the disturbance behaviour at lower speeds, a load torque step to half the rated torque is shown in Fig. 10. The speed setpoint is $\hat{n}^{*}_{\mathrm{mech}} = 400\,^{1}/_{\mathrm{min}}$ and the dynamic response is on the higher level (cf. Table II). Although the system remains stable in steady state at full load torque, a step up to this value leads to very low speeds, so that the system is not stable for a short time, meaning that this test can't be shown here.
The lower speed limit is more than sufficient for stable operation of the SSC, as the anisotropy-based method is used below 10 % of the rated speed.

## Conclusions

This paper presents a novel structure for rotor position estimation in PMSMs at higher speeds. The method based on the voltage equation evaluates the current slopes within a PWM period and minimises the rotor position estimation error within a control cycle. High dynamics and stability were demonstrated over the range of constant flux of the machine and validated by experimental results.

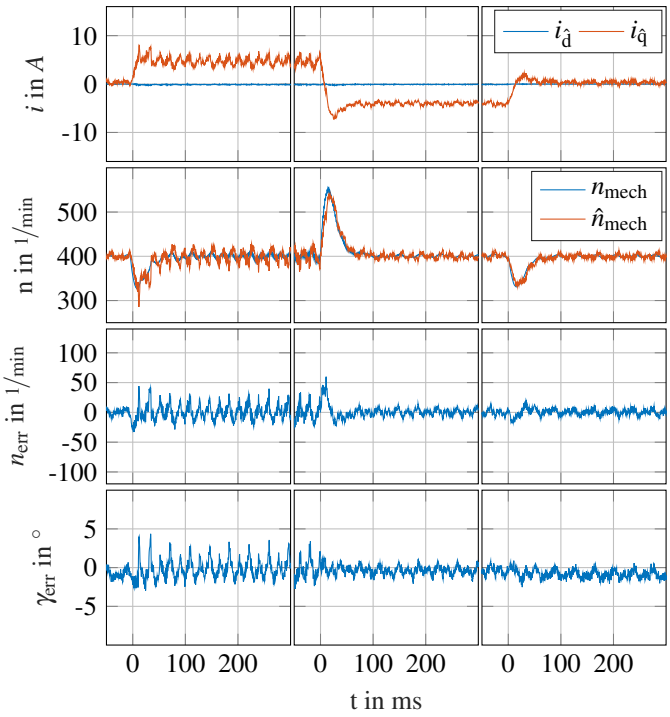


Fig. 9: Investigation of the low speed limit at 400 1/min speed setpoint. 0.5 of rated torque is applied (left), reversed (centre) and reduced to zero (right)

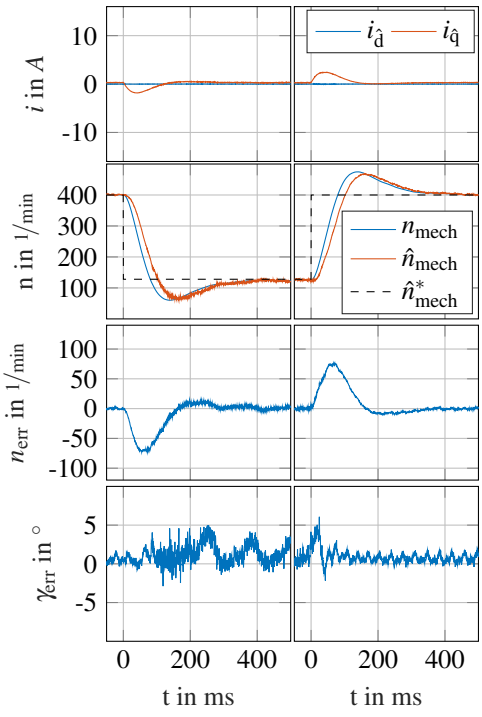


Fig. 10: Investigation of the low speed limit at idle with reduced dynamic response. Speed setpoint $\hat{n}^*_{mech}$ is reduced to 128 1/min and increased to 400 1/min

# References


[1] S.-K. Sul and S. Kim, "Sensorless Control of IPMSM: Past, Present, and Future," *IEEJ Journal of Industry Applications*, vol. 1, no. 1, pp. 15–23, 2012.

[2] D. Paulus, J.-F. Stumper, P. Landsmann, and R. Kennel, "Robust encoderless speed control of a synchronous machine by direct evaluation of the back-EMF angle without observer," in *2010 First Symposium on Sensorless Control for Electrical Drives*, Jul. 2010, pp. 8–13.

[3] Z. Chen, M. Tomita, S. Doki, and S. Okuma, "An extended electromotive force model for sensorless control of interior permanent-magnet synchronous motors," *IEEE Transactions on Industrial Electronics*, vol. 50, no. 2, pp. 288–295, Apr. 2003.

[4] N. Himker, G. Lindemann, K. Wiedmann, B. Weber, and A. Mertens, "A Family of Adaptive Position Estimators for PMSM Using the Gradient Descent Method," *IEEE Journal of Emerging and Selected Topics in Power Electronics*, pp. 1–1, 2021.

[5] N. Himker, G. Lindemann, and A. Mertens, "Iterative Tracker for Anisotropy-Based Self-Sensing Control of PMSM," in *2019 IEEE 10th International Symposium on Sensorless Control for Electrical Drives (SLED)*, Sep. 2019.

[6] G. Lindemann, N. Himker, and A. Mertens, "Enhanced Observer with Adaptive Reference Frame for Self-Sensing Control of PMSM," in *2019 IEEE 10th International Symposium on Sensorless Control for Electrical Drives (SLED)*, Sep. 2019.

[7] Y. Duan and M. Sumner, "A novel current derivative measurement using recursive least square algorithms for sensorless control of permanent magnet synchronous machine," in *Proceedings of The 7th International Power Electronics and Motion Control Conference*, vol. 2, Jun. 2012, pp. 1193–1200.

[8] P. Landsmann, J. Jung, M. Kramkowski, P. Stolze, D. Paulus, and R. Kennel, "Lowering injection amplitude in sensorless control by means of current oversampling," in *Sensorless Control for Electrical Drives (SLED), 2012 IEEE Symposium On*, Sep. 2012, pp. 1–6.

[9] S. Kim, J. I. Ha, and S. K. Sul, "PWM Switching Frequency Signal Injection Sensorless Method in IPMSM," *IEEE Transactions on Industry Applications*, vol. 48, no. 5, pp. 1576–1587, Sep. 2012.

[10] K. Wiedmann and A. Mertens, "Novel MRAS approach for online identification of key parameters for self-sensing control of PM synchronous machines," in *2012 15th International Power Electronics and Motion Control Conference (EPE/PEMC)*. Novi Sad, Serbia: IEEE, Sep. 2012, pp. LS4b–1.2–1–LS4b–1.2–8.

[11] P. Landsmann, "Sensorless Control of Synchronous Machines by Linear Approximation of Oversampled Current," Ph.D. dissertation, Technische Universität München, 2014.

[12] B. Weber, G. Lindemann, and A. Mertens, "Reduced observer for anisotropy-based position estimation of PM synchronous machines using current oversampling," in *Proc. IEEE Int. Symp. Sensorless Control for Electrical Drives (SLED)*, Sep. 2017, pp. 121–126.

[13] S. P. Boyd and L. Vandenberghe, *Convex Optimization*. Cambridge, UK ; New York: Cambridge University Press, 2004.

[14] B. Weber, T. Brandt, and A. Mertens, "Compensation of switching dead-time effects in voltage-fed PWM inverters using FPGA-based current oversampling," in *2016 IEEE Applied Power Electronics Conference and Exposition (APEC)*, Mar. 2016, pp. 3172–3179.